Available online at www.sciencedirect.com

SciVerse ScienceDirect

Ceramics International 39 (2013) 1695–1705

CERAMICS INTERNATIONAL

www.elsevier.com/locate/ceramint

Antibacterial studies on Eu–Ag codoped TiO_2 surfaces

S. Ramya, S.D. Ruth Nithila, R.P. George, D.Nanda Gopala Krishna, C. Thinaharan, U. Kamachi Mudali*

Corrosion Science and Technology Group, Indira Gandhi Centre for Atomic Research, Kalpakkam 603102, India

Received 17 May 2012; received in revised form 26 July 2012; accepted 6 August 2012
Available online 21 August 2012

Abstract

The photocatalytic property of titanium dioxide is well known and is responsible for its antimicrobial activity. The present study is focused on the understanding of enhanced antimicrobial property of Eu–Ag codoped TiO_2 surfaces, which were prepared using the sol–gel method. After exposing Eu–Ag codoped TiO_2 surfaces to *Pseudomonas aeruginosa*, the microbes attached on them were characterized by total viable counts, epifluorescence and Raman microscopic experiments. These techniques confirmed the effective reduction of microbial attachments on Eu–Ag codoped surfaces when compared to the control and Eu doped TiO_2 surfaces. The reason was that the co-dopants favored the transformation of anatase/rutile mixed phase and led to the increase in photocatalytic activity of the Eu–Ag codoped TiO_2 surfaces. Also, the metallic silver on TiO_2 surface enhanced the photoactivity by accelerating the transport of photogenerated electrons to oxygen molecules, preventing the electron–hole recombination and facilitating the activity of codoped surfaces.

Keywords: A. Sol–gel processes; B. Surfaces; C. Chemical properties; D. TiO_2

1. Introduction

Titanium dioxide (TiO_2) is well known for its semiconductivity, photocatalysis and non-toxicity [1,2]. Due to its excellent photocatalytic activity, the material has gained enormous attention and become the subject of contemporary research interest [3–15]. There are many literatures on doping of TiO_2 in the recent years [16–27]. Most of them discussed about the reduction in the possible electron–hole recombination and higher photocatalytic activity [16–18]. It was proved that the dopant particles of nanosize gave improved catalytic behavior, and was used for the degradation of many compounds and this peculiar quality lead to enhanced antimicrobial property of doped TiO_2 surfaces [16]. Added to this, co-doping has also been used to reduce the band gap energies, which shifted the absorption to longer wavelengths when exposed to visible light, leading to higher catalytic and microbial activities [14,28–32].

In the recent past, researchers contributed a lot toward the lanthanide doping of TiO_2 [33–38]. It was reported that the f-orbital of lanthanide ions interact with the Lewis bases and form complexes with unique electronic structure $4fx5dy$ and oxygen vacancies [16,37,38] and hence, the incorporation of lanthanide ions in a TiO_2 matrix became easier [37–40]. In analogous to the earlier reports in this area, we have carried out an investigation on antimicrobial properties of Eu–Ag codoped TiO_2 surfaces. For the sake of fundamental scientific interest and to get an insight, antibacterial properties of Eu doped TiO_2 and Eu–Ag codoped TiO_2 surfaces were compared by us. We adopted the same concept and methodology presented in our earlier paper on antimicrobial characterization of anodized and sol–gel TiO_2 surfaces [41]. For the present analysis, the codoped surfaces were produced using the sol–gel method since the method was considered easy and adoptable. The coated surfaces were characterized by Raman spectroscopy, photoluminescence, X-ray photoelectron spectroscopy and X-ray diffraction techniques. The antimicrobial effects were tested with *Pseudomonas aeruginosa*. The microbes attached on the doped and codoped surfaces

*Corresponding author. Tel./fax: +91 44 27480121.
E-mail address: kamachi@igcar.gov.in (U. Kamachi Mudali).

0272-8842/$ - see front matter © 2012 Elsevier Ltd and Techna Group S.r.l. All rights reserved.
http://dx.doi.org/10.1016/j.ceramint.2012.08.012

were characterized by total viable counts, epifluorescence and Raman microscopic experiments.

2. Materials and methods

2.1. Control titanium specimens

Commercially pure titanium Grade-2 samples were used in this study. The surface cleaning of the metal and the sample preparation was done as reported in our earlier study [41]. The Ti coupons of size $30 \times 20 \times 1$ mm^3 were cut and treated in an acid bath (HNO_3, 400 g/l + HF, 40 g/l + water) to remove any surface scales present. The treated specimens were then cleaned ultrasonically in acetone, washed in flowing water and finally rinsed in distilled water and air-dried. These specimens were used as a control to compare the photocatalytic activity of the Eu-doped and Eu–Ag codoped TiO_2 specimens.

2.2. Eu-doped and Eu–Ag codoped TiO_2 sol–gel coated titanium specimens

In our experiments, all reagents used for the preparation of TiO_2 sol–gel were of AR grade. The Eu–TiO_2 sol–gel was prepared as reported in the literature [42]. The Eu–TiO_2 sol was prepared from tetra-*n*-propyl titanate and ethyl acetoacetate (EAcAc), a chelating agent. Initially, 40 ml of ethanol and 2 ml of EAcAc were mixed, followed by the addition of 4 ml of tetra-n-propyl titanate. Tetra-n-propyl titanate: EAcAc: $Eu(NO_3)_3 \cdot 6H_2O$:C_2H_5OH with molar ratios 1:4:0.1:27, were stirred continuously for 1 h at 50 °C. After 30 min, 0.2 ml distilled water was carefully added to the solution to initiate the hydrolysis of tetra-n-propyl titanate. The obtained transparent yellow solution was kept stirring for 10 h. The yellow transparent solution was aged for 24 h before coating on the metal surface. For the preparation of Eu–Ag codoped TiO_2, silver nitrate was also added along with the Europium nitrate solution. The ratio of Eu^{3+} and Ag^{+} as 1:1 was maintained in the codoped TiO_2. The titanium specimens were ground with no. 320–1000 SiC emery papers gradually, polished and then ultrasonically cleaned in acetone and distilled water for 10 min, respectively. After hot air drying, they were coated with doped and codoped TiO_2 coatings by the dip-coating method. After drying naturally in the ambience, the specimens were heated in an oven at 150 °C for 30 min. The process was repeated for 4–5 times to increase the coating thickness. Then, the samples were heat-treated at 470 °C for 2 h to enable the oxide conversion.

2.3. Characterization of Eu-doped and Eu–Ag codoped TiO_2 sol–gel coated titanium specimens

2.3.1. Raman and photoluminescence spectroscopy

All the sol–gel coated specimens were characterized using Raman, photoluminescence (PL) spectroscopic techniques. Both Raman and PL spectra were recorded by an integrated Raman microscope (HR800, Jobin Yvon) equipped with 1800 grooves/ mm holographic grating. An argon ion laser of 488 nm and 10 mW power was used as an excitation source for recording Raman and PL spectra of control, Eu-doped and Eu–Ag codoped TiO_2 sol–gel coated Ti surfaces. The system consists of an Olympus optical microscope mounted at the entrance of the Raman spectrograph and the 10 × long distance objective was used to focus the beam on the sample. The laser spot size was approximately 3 μm and the slit width was 400 μm. The back scattered Raman spectra were recorded using super cooled (< -110 °C) 1024×256 pixels CCD detector. All the Raman spectra were collected with 5 s exposure time and 20 accumulations. PL spectra of all the samples were recorded with 30 s exposure time and 5 accumulations.

2.3.2. X-ray photoelectron spectroscopy (XPS)

X-ray photoelectron spectroscopy (XPS) experiments were carried out using a PHOIBOS 150 spectrometer employing monochromatic Al K_α (1486.74 eV) as the primary source radiation at room temperature. The anode was operated at a voltage of 13 kV and source power level was set to 300 W. The spectra were collected using the PHOIBOS 150 MCD-9 analyzer with a resolution of 0.67 eV for 656 kcps at pass energy of 10 eV and analyzed using the Casa XPS software. The binding energies were calculated with respect to the C1s = 284.8 eV [43]. The analysis of each of the elemental peak is deconvoluted after the subtraction of background of the Shirley type. For the deconvolution of elemental peak of europium linear background subtraction was used.

2.3.3. X-ray diffraction studies (XRD)

The crystalline phases of doped and codoped TiO_2 nanoparticles were analyzed by X-ray diffraction (XRD) measurements which were carried out at room temperature by using a Siemens X-ray diffraction D500 with Cu K_α radiation.

2.4. Evaluation of antimicrobial activity of modified surfaces

Exposure studies and post-exposure analysis were done by adapting the similar procedure reported in our earlier paper [41] for comparing microbial attachment of control, Eu doped and Eu–Ag codoped TiO_2 surfaces.

2.4.1. Laboratory exposure studies

The Eu doped and Eu–Ag codoped TiO_2 sol–gel coated titanium specimens were exposed to the culture of *P. aeruginosa* bacteria in 10% nutrient broth in the cylindrical glass vessel containing the appropriate exposure medium. The specimens were withdrawn after 72 h for antibacterial studies.

2.4.2. Post-exposure studies

2.4.2.1. Total viable count estimation (TVC). All the specimens exposed to *P. aeruginosa* were removed after

72 h exposure and gently washed to remove out loosely adhering cells. The microbes on the 3 sets of specimens were dispersed into 15 ml of sterile phosphate buffer (0.0425 g KH_2PO_4, 0.19 g $MgCl_2$/l) using a sterile brush. Serial dilutions of the biofilm suspensions were prepared and 0.1 ml of each dilution was plated onto zobell marine agar (ZMA) from Hi media M384. The plates were incubated for 24–48 h at 32 °C, and the TVC was determined [41,44], and its statistical analysis was performed by the MYSTAT software.

2.4.2.2. Epifluorescence microscopic studies. The specimens of control, doped and codoped TiO_2 were exposed to *P. aeruginosa* for bacterial growth and used for direct microscopic observation using epifluorescence microscopy [41,45]. The specimens were gently washed with sterile water, and air-dried in a sterile chamber, and then the surface was flooded using 0.1% acridine orange. The excess stain was drained off after 2 min, and the specimens were washed in sterile water, dried and observed under a Nikon Eclipse E600 epifluorescence microscope (excitation filter BP 490; barrier filter O 515). When the intercalation of acridine orange with DNA and RNA was taking place, either green or red fluorescence was observed upon 480–490 nm excitations.

2.4.2.3. Raman protocol for antimicrobial studies. The titanium coupons with the bacterial biofilms were immersed in the Ag colloidal suspensions and their analysis in the Raman microscopic scanning mode were carried out with the same HR800 Jobin Yvon Raman spectrometer using 1800 grooves/ mm holographic grating. He–Ne laser of 633 nm was used as an excitation source. The laser spot size was approximately 3 μm and laser power was 5 mW at the sample. The back scattered Raman spectra were recorded using super cooled (< -110 °C) 1024×256 pixels CCD detector over the range 80–4000 cm^{-1}. All the spectra were collected with 5 s integration and 20 accumulations. Both integration time and number of accumulations were kept constant for all the experiments. The spectral maps were obtained by collecting spectra over 100×100 μm^2 area with 5 s exposure time and 20 CCD accumulations. Data acquisition was done by an associated software package.

3. Results and discussion

3.1. Characterization of Eu-doped and Eu–Ag codoped sol–gel TiO_2 coated Ti specimens

3.1.1. Raman, X-ray diffraction and photoluminescence analysis

The coated titanium coupons were characterized using Raman spectroscopic experiments. Both Eu doped and Eu–Ag codoped gave Raman signatures of TiO_2 at the surface. Generally, the presence of anatase TiO_2 was confirmed by its characteristic Raman modes at 142 (E_g), 393 ($B1_g$), 636 (E_g) cm^{-1} whereas the rutile phase was confirmed by its Raman modes at 238, 445 and 609 cm^{-1} [46]. Fig. 1(a and b) depicted the Raman spectra of control and Eu doped TiO_2 coupons. Raman spectra were collected at randomly selected points (at least 5) of each sample, and were observed to be reproducible. This was achieved by the XY motorized sample stage in the Raman microscope. Fig. 1(c and d) shows the Raman spectra taken from 2 different positions at Eu–Ag codoped TiO_2 coupons. The Raman spectra taken at different places of Eu–Ag codoped TiO_2 coupons indicated the presence of both anatase and rutile phases (Fig. 1(c and d)). The spectral assignments and the interpretation were made based on the literature [46–49]. The Eu doped TiO_2 surface showed predominant anatase phase. In the case of Eu–Ag codoped surface, the intensity of the peak at 145 cm^{-1} was drastically reduced whereas new peaks at 249, 447, 612 cm^{-1} were observed due to anatase to rutile transformation [48]. Peak positions were slightly altered from the reported values as a result of surface inhomogeneities and particle size effects. Few extra peaks were observed owing to the aggregation of small particles and surface effects. Generally, Eu-doped TiO_2, gave stable anatase phase, though the annealing temperatures were up to 700 °C, the anatase to rutile phase was not formed [48]. Due to the existence of Eu–O–Ti bonding in Eu doped TiO_2 substrate, the annealing temperature was increased for the anatase–rutile transformation [48]. The Eu^{3+} ion will prefer to occupy interstitials because of the difference in ionic radii of the both Eu^{3+} and Ti^{4+} and block the rutile formation [48,49]. Hence, the presence of anatase phase in the Raman spectra of Eu doped TiO_2 was very much supported by this fact. However, the incorporation of Ag into the Eu doped TiO_2 matrix, stimulate the anatase to rutile transformation and the Raman spectra of Eu–Ag codoped surface

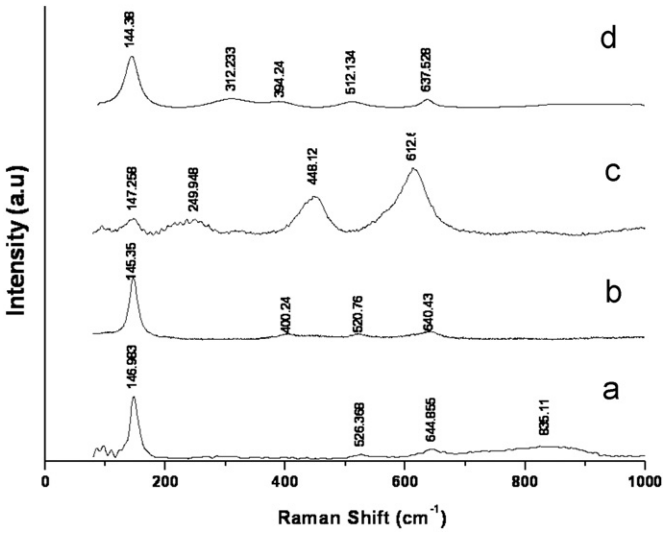

Fig. 1. Raman spectra taken from the (a) control (b) Eu-doped and (c, d) Eu–Ag codoped TiO_2 coated surfaces. Excitation wavelength = 488 nm; laser power = 10 mW; exposure time = 5 s; laser acquisitions = 20.

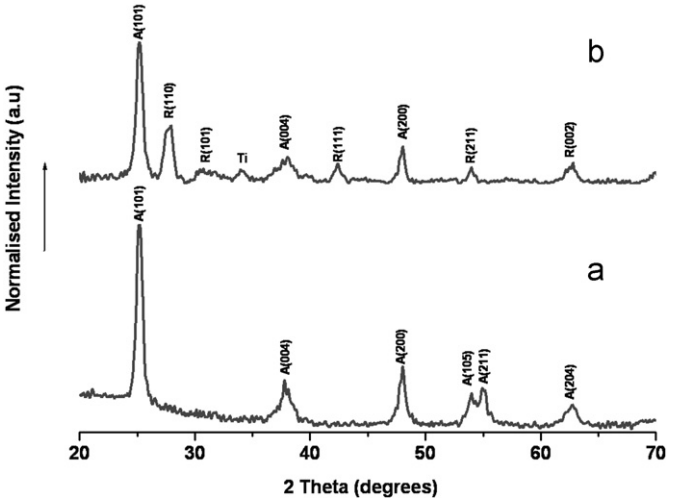

Fig. 2. X-ray diffraction pattern of (a) Eu-doped and (b) Eu-Ag codoped TiO_2 coated surfaces.

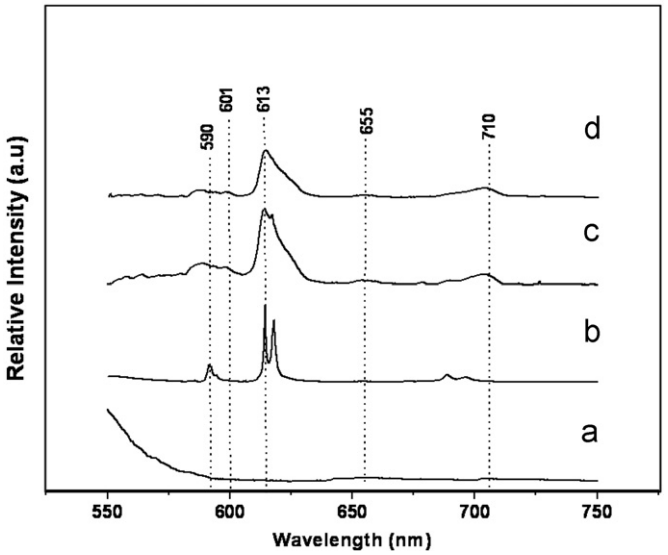

Fig. 3. Photoluminescence spectra taken from the (a) control, (b) europium nitrate, (c) Eu-doped and (d) Eu–Ag codoped TiO_2 coated surfaces. Excitation wavelength = 488 nm; laser power = 10 mW; exposure time = 30 s; laser acquisitions = 5.

indicated the formation of clear anatase/rutile mixed phase. The results were in good agreement with the X-ray diffraction experiments (Fig. 2). The crystallite size was calculated by the Debye–Scherrer formula $D = K\lambda/\beta\cos\theta$, where D is the crystallite size, λ is the wavelength of X-ray radiation (0.154 nm), K is the constant (0.89), θ is the Bragg's angle and β is the peak width at half maximum height after subtracting the equipment broadening [39,50]. It was found that the average crystallite sizes of Eu doped and Eu–Ag codoped TiO_2 surfaces were 11 and 10 nm, respectively. The crystallite sizes were calculated by considering (101) plane of anatase of doped and codoped surfaces. In addition to that, the crystallite size of Eu–Ag codoped TiO_2 surface was calculated (14 nm) with regard to the 110 plane of rutile phase. It is well known that the decrease in crystallite size will increase the microstrain in the sample, and the Eu and Ag atoms will be just adsorbed on the surface [39,50]. The microstrain was calculated using the formula, $\beta/4\tan\theta$ [50] and observed to be 0.013 and 0.014 for Eu doped and Eu–Ag codoped TiO_2 surfaces, respectively. By using XRD, the weight content of [51] anatase and rutile phase in Eu–Ag codoped TiO_2 was determined using the formula

$$WR = 1/1 + 0.8(IA/IR), \quad (1)$$

$$WA = 1\text{-}WR, \quad (2)$$

where WA and WR are the weight fraction of anatase and rutile, IA and IR are the diffraction peak intensities of anatase (101) and rutile (110), respectively. The calculated weight contents of anatase and rutile in codoped surface were 0.67 and 0.33 respectively. The crystal planes (101) and (200) of the anatase phase were selected to calculate the lattice parameters of the Eu-doped and Eu–Ag codoped TiO_2 surfaces. The lattice parameter and unit cell volume of the samples were calculated by using the formula [52] $d(hkl) = \lambda/2\sin\theta$ (Bragg's law) and $d(hkl) = \left(h^2/a^2 + k^2/a^2 + l^2/c^2\right)^{-1/2}$ where hkl are the Miller indices; a, b and c are the lattice parameters (in a tetragonal system, $a = b \neq c$); $d(hkl)$ is the interplanar spacing between the crystal planes (hkl); λ is the X-ray wavelength; and θ is the diffraction angle. The lattice parameters for Eu-doped TiO_2 surfaces were found to be $a = 0.3785$ nm; $c = 0.9484$ nm and slight deviation was shown from the lattice parameter values of codoped TiO_2 surfaces ($a = 0.3786$ nm and $c = 0.9509$ nm). The cell volume was also calculated and observed to be higher for Eu–Ag doped TiO_2 (0.1363 nm^3) than that of Eu doped TiO_2 (0.1358 nm^3) due to the incorporation of Ag into the TiO_2 matrix.

Fig. 3 shows photoluminescence spectra of control, Eu-doped and Eu–Ag codoped Ti surfaces at room temperature. Our Instrument (HR800, Jobin Yvon) was not provided with UV laser probe to record the PL spectra. Hence, the emission spectra were recorded after exciting the samples at 488 nm. There was no specific reason in selecting this particular excitation wavelength for PL experiments. Fig. 3(c and d) showed emission peaks at 590 and 614 nm, which were due to magnetic (5D0 → 7F1) and electrical (5D0 → 7F2) dipole transitions respectively [47]. The PL spectra indicated the presence of europium ions in the doped and codoped surfaces. The emission spectra of doped and codoped surfaces consists emission lines at 591, 600, 613, 660 and 710 nm due to Eu^{3+} ion transitions from $^5D_0$ to ^7F_J ($J = 0$, 1, 2, 3 and 4) [47,53]. The possibility of formation of $Eu_2Ti_2O_7$ was eliminated due to the presence of peaks at 591 and 613 nm [47]. The intensities of electrical dipole were higher than that of magnetic dipole transitions. The asymmetric factor of the europium ion in the TiO_2 matrix was calculated by finding out the ratio of the electric to the magnetic dipole transitions [47,54,55]. The values of asymmetric factor of Eu doped and Eu–Ag codoped surfaces were found to be

3.45 and 3.39, respectively. Though ratio of electric to magnetic dipole transitions were almost same, the intensity of electrical dipole transition was decreased upon codoping due to the cross relaxation among europium and silver ions [54]. As reported in earlier literature, an unusual increase in the intensity of the electrical dipole transitions was observed due to polarizability effect of the host matrix [54,55].

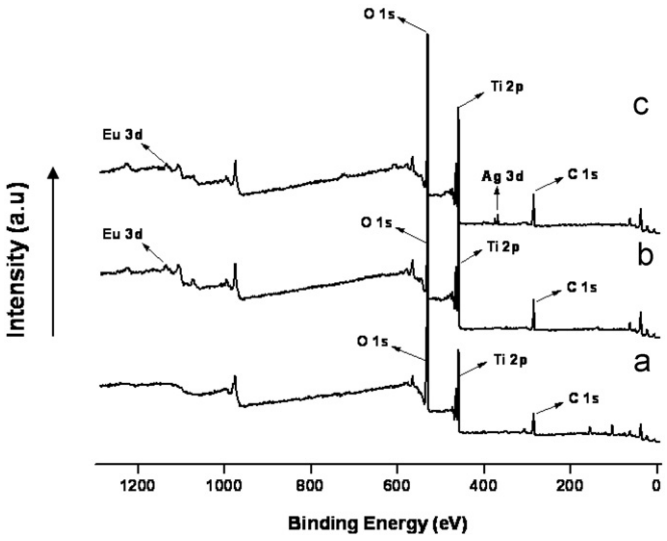

Fig. 4. XPS survey spectra of (a) control, (b) Eu-doped and (c) Eu–Ag codoped TiO_2 coated surfaces.

3.1.2. X-ray photoelectron spectroscopy analysis

The XPS survey spectrum clearly revealed the presence of O1s (530.3 eV), Ti 2p, and Ag 3d (Fig. 4). The XPS analysis of coated surfaces showed distinct peaks corresponding to Ti^{4+} and Eu^{3+} and Ag^0 [43]. However, Eu was observed with very low intensity indicating the lesser atom content of europium. The existence of titanium as Ti^{4+} was confirmed by the presence of peak at 459.2 eV [43]. No binding energy peaks corresponding to Ti^{2+} or Ti^{3+} were observed at 455.1 eV [43] and 457.7 eV [47], and hence the possibility of occurrence of Ti^{2+} or Ti^{3+} was ruled out. The observed binding energy values O1s and Ti 2p were slightly shifted to higher values due to the incorporation of dopants [40,47]. The formation of Eu–O–Ti chemical bond was confirmed by the increase in binding energy values [47]. The high resolution scan (Figs. 5 and 6) of the $3d_{5/2}$ core level of Eu revealed two distinct peaks around 1135.4 eV and 1127.0 eV denoting Eu (III) and Eu (II), respectively, for both Eu-doped and Eu–Ag codoped surfaces [40,56]. When the high resolution scan for 3d core level of Ag was carried out for Eu–Ag codoped surfaces, two well separated peaks were observed at 368.8 eV and 374.8 eV [37] with a peak separation of 6 eV, inferring the presence of metallic Ag in the codoped Ti surfaces.

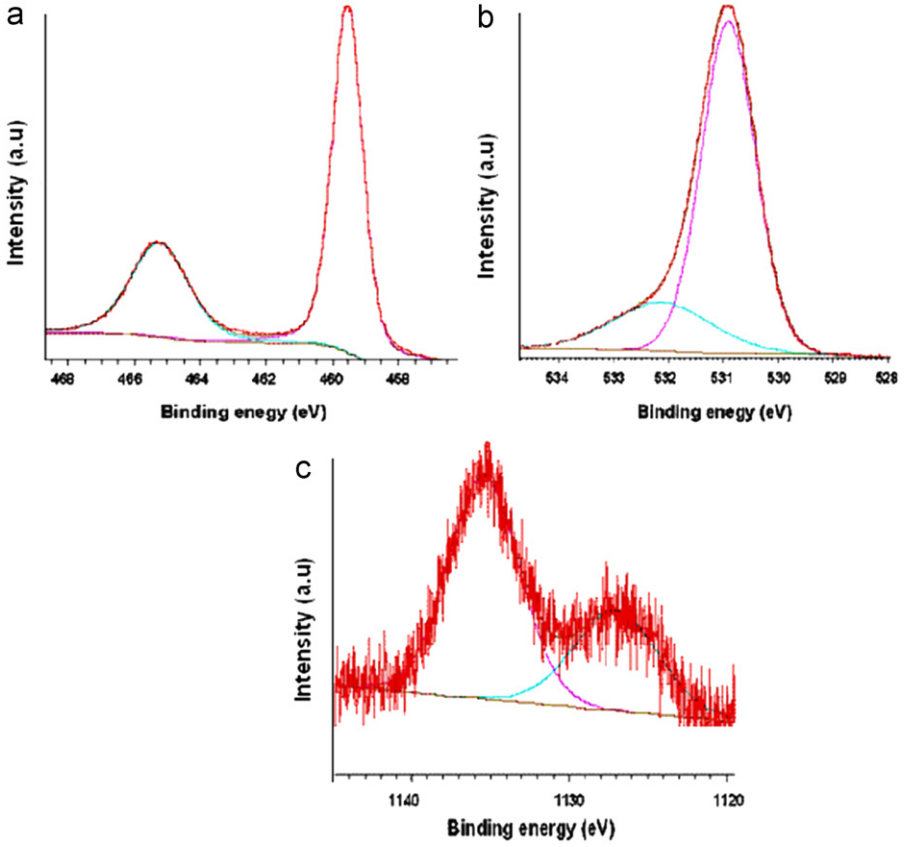

Fig. 5. High resolution XPS spectra of Eu-doped TiO_2 coated surfaces: (a) Ti 2p; (b) O 1s and (c) Eu $3d_{5/2}$ core levels.

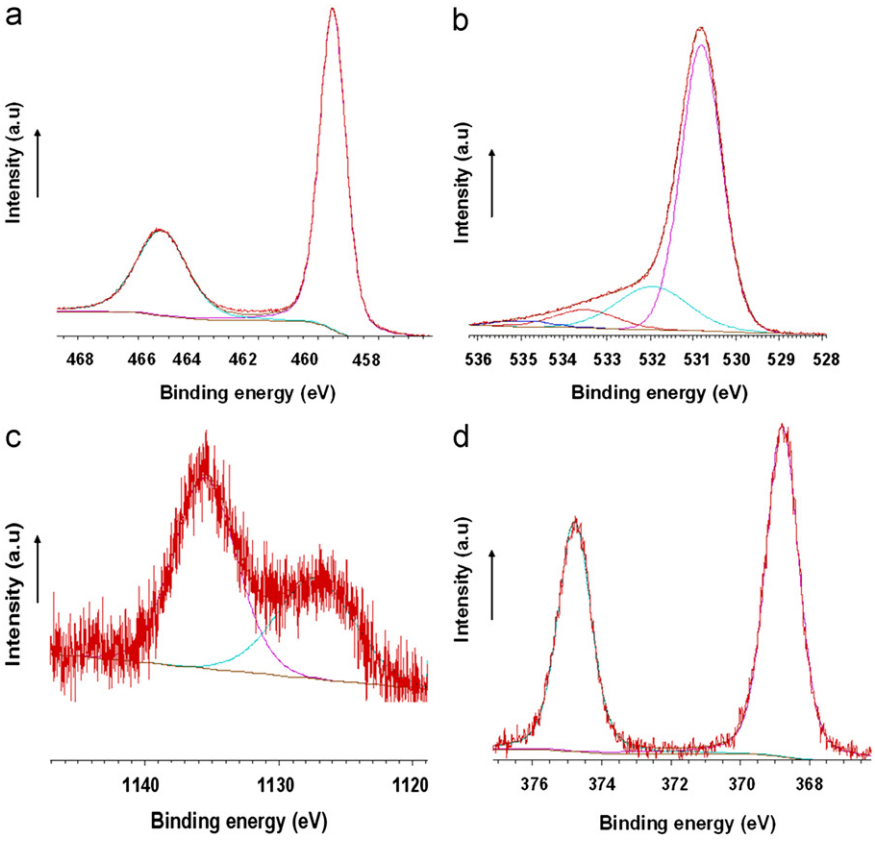

Fig. 6. High resolution XPS spectra of Eu–Ag codoped TiO_2 coated surfaces: (a) Ti 2p; (b) O 1s; (c) Eu $3d_{5/2}$ and (d) Ag 3d core levels.

3.2. Characterization of bacterial biofilms formed on control, Eu doped and Eu–Ag codoped titanium specimens

The control, Eu doped and Eu–Ag codoped sol–gel coated titanium coupons were exposed to *P. aeruginosa* and retrieved after 72 h. The bacterial biofilms formed on the exposed sol–gel coated Ti surfaces were characterized using the following techniques and the results are discussed below:

3.2.1. Total viable count (TVC)

Fig. 7 shows the total viable counts (TVC) of all the microorganisms and it was observed that TVC counts in the Eu–Ag codoped titanium surface were 4 order lesser than that of control surfaces.

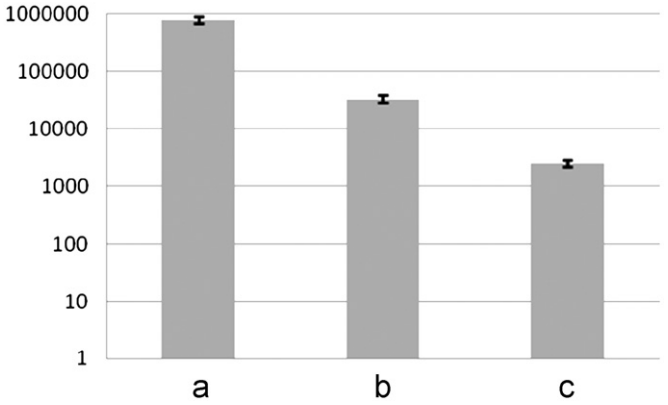

Fig. 7. TVC count in the (a) control, (b) Eu-doped and (c) Eu–Ag codoped TiO_2 coated surfaces.

3.2.2. Epifluorescence microscopic observation

Epifluorescence studies showed the morphology of microbes formed on different titanium surfaces exposed to *P. aeruginosa*. Acridine Orange (AO) is a nucleic acid selective metachromatic dye, which differentially stains RNA and DNA. It fluoresces in orange when interacted electrostatically with RNA and in green while intercalated with DNA. Since the metabolically active cells are rich in RNA, the dye prefers to bind with RNA and fluoresces in orange. On the contrary, metabolically inactive cells have very less RNA content, the intercalation of the dye with DNA is favored and hence green fluorescence is observed. Thus, the number of orange fluorescing cells represented the actively metabolizing cells, and the green fluorescing cells indicated the photocatalytically inactivated microbial cells on Ti specimens [41]. Fig. 8(b and c) showed that Eu doped and Eu–Ag codoped TiO_2 coated titanium samples had lesser biofilm formation than control specimens (Fig. 8a). In our studies, the biofilm formation was always patchy and non-uniform. However, the epifluorescence image of microbes on Eu–Ag codoped specimen showed lesser distribution of bacterial film than Eu doped and

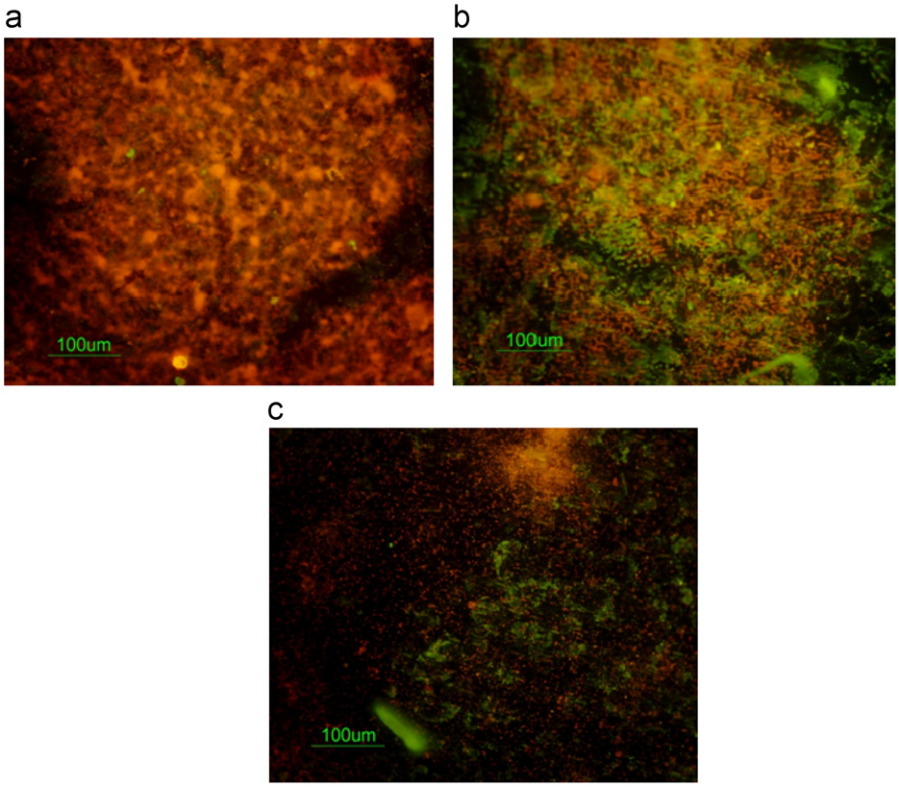

Fig. 8. Epifluorescence microscopic images of biofilms on (a) control (b) Eu-doped and (c) Eu–Ag codoped TiO_2 coated surfaces, which were earlier exposed to *P. aeruginosa* and retrieved after 72 h.

control surfaces. The results of epifluorescence microscopic studies were in good agreement with the TVC experiments.

3.2.3. Surface enhanced Raman spectroscopic experiments of control, Eu doped and Eu–Ag codoped Ti surfaces

The microbial characterization on Ti surfaces using Raman spectroscopy has been already reported by us elsewhere [41,57]. Similar methodology was adapted in the present study for analyzing the Raman spectra. As expected, normal Raman experiments (NR) on the bacterial biofilms on different titanium surfaces gave unclear spectra. Hence, the surface enhanced Raman scattering (SERS) was used to enhance the signal intensity and resolution. Different regions of the titanium coupons containing bacterial biofilms were analyzed using Raman microscopy. The micro-SERS spectra on the biofilms on titanium surfaces using Ag colloid were higher in magnitude than that of NR experiments. The Ag colloid was synthesized as stated in the literature [58]. A tentative assignment of bands (Table 1) was performed by referring to Raman and SERS assignments for *P. aeruginosa* from literature [59–61]. The characteristic Raman frequencies of the cellular components were used to confirm the presence of microbial attachments. Fig. 9(a, b and c) shows the Raman spectra of *P. aeruginosa* on control, Eu doped and Eu–Ag codoped titanium surfaces, respectively. All the spectra showed similarities and indicated considerable microbial attachment. Fig. 10(a, b and c) depicted the light microscopic image of *P. aeruginosa* biofilm on control, Eu-doped and Eu–Ag codoped sol–gel coated Ti specimens, respectively.

Table 1
Tentative peak assignments (cm^{-1}) for micro-SERS spectra of *P. aeruginosa* [58–60] on different sol–gel coated titanium specimens in Ag colloid. Wavelength of excitation is 633 nm.

Band (cm^{-1})	Assignments
593	Carbohydrates
646, 684, 669	COO^- bending and C–C skeletal
735	Ring I deformation
803, 869, 824, 884	Different C–N stretching from proteins
1016, 1021, 1076	Polysaccharides and C–C, C–O, C–O–H deformation
1170, 1172, 1177	Aromatic amino acids in proteins
1256, 1269	N–H, C–N, amide III (protein)
1350, 1360, 1373, 1381, 1387	C–H bending of protein, COO^- symmetric stretching, various bending and stretching of proteins.
1404, 1461	COO^- symmetric stretching
1584	C=C lipid
1635	Amide I
Other small peaks	Unassigned

The Raman spectral maps (Fig. 11(a–c)) were obtained by collecting the spectra with 5 s exposure time over $100 \times 100\ \mu m^2$ area on the bacterial biofilms on different Ti surfaces. The maps were obtained by considering the

protein vibrations. Generally, Raman map gives the intensity distributions of one particular spectral range from which the changes in the composition of a specific component can be determined. The intensity variations of specific components over $100 \times 100\ \mu m^2$ area is depicted in the form of colored Raman image. Since proteins are one of the major constituents of the bacterial biofilm, their distributions were expected to give the measure of biofilm density at the surface. Hence, Raman maps of proteins (Fig. 11(a–c)) were taken at various titanium surfaces. In Fig. 11, pinkish white and black color regions indicated the lesser and higher intensities, respectively (color scale is mentioned in the figure). The intensities of the Raman maps are related to the surface composition and thickness of the biofilm. In the present study, the mapping experiments undoubtedly showed the lesser distribution of microbes, inferring the decrease of microbial attachments on Eu–Ag codoped and Eu-doped TiO_2 coated titanium surfaces.

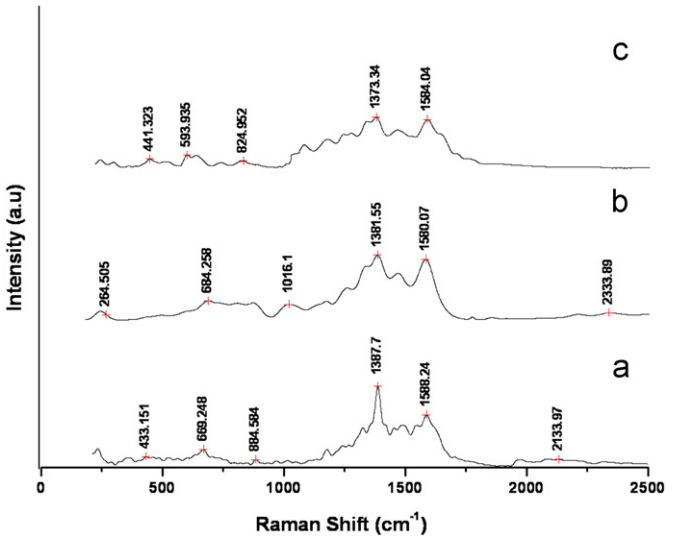

Fig. 9. The Raman spectra taken from the *P. aeruginosa* on (a) control, (b) Eu-doped and (c) Eu–Ag codoped TiO_2 coated Ti surfaces. Excitation wavelength = 488 nm; laser power = 10 mW; exposure time = 5 s; Laser acquisitions = 20.

The mapping of proteins (Fig. 11(a–c)) was carried from 1300 to 1400 cm^{-1} (various stretching and bending of proteins) [59–61]. The mapping experiments were repeated for other spectral regions. The observed results were reproducible and in good agreement with the earlier findings. Different regions of the sol–gel coated specimens showed lesser bacterial distribution than that of control specimens. An effective microbial reduction was observed for Eu–Ag codoped samples than other Ti surfaces. The observed Raman results were in well agreement with the epifluorescence microscopy and TVC results.

Generally, smaller the crystal size of the particles larger is the surface area with more photochemical activity. Since the particles sizes of both doped and codoped TiO_2 surfaces were almost same, it was expected to have similar

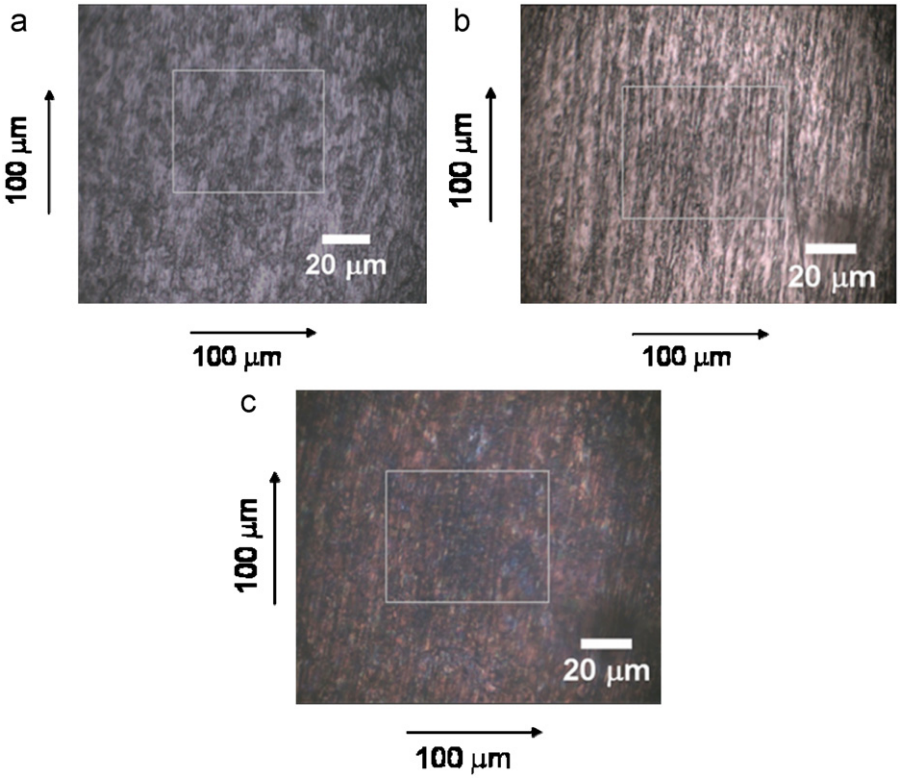

Fig. 10. The light microscopic image of *P. aeruginosa* biofilm on (a) control, (b) Eu-doped and (c) Eu–Ag codoped TiO_2 coated Ti specimens. The image was obtained by Olympus Raman microscope using 10× long distance objective. The square box inside the figure represents the selected region of interest where Raman mapping was carried out.

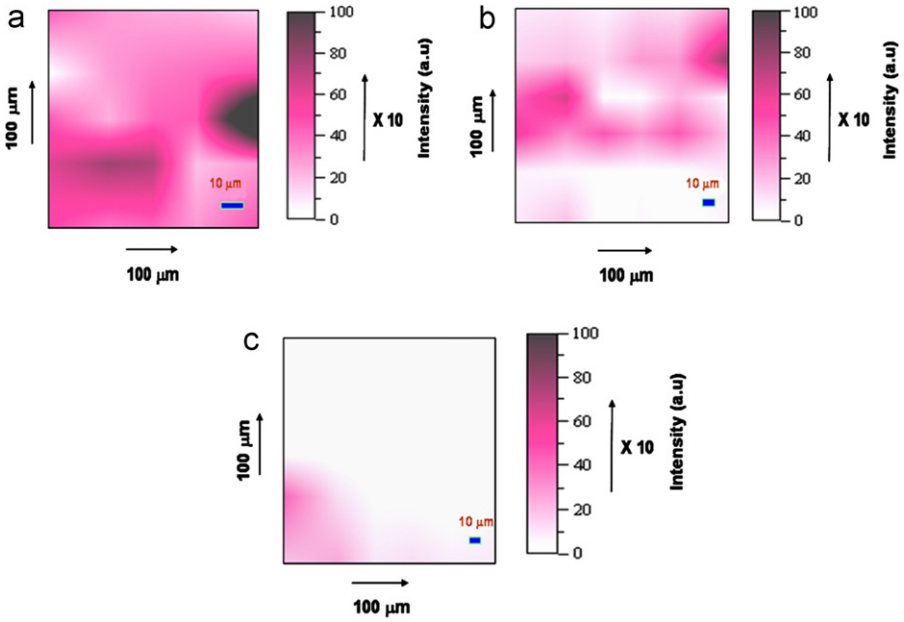

Fig. 11. Distribution of proteins in the biofilms formed on (a) control, (b) Eu-doped and (c) Eu–Ag codoped Ti specimens. Raman map was recorded from 1300 to1400 cm^{-1}, corresponds to various bending and stretching of proteins. (For interpretation of the references to color in this figure, the reader is referred to the web version of this article.)

photocatalytic behavior from those surfaces. Conversely, Eu–Ag codoped TiO_2 surface was shown to be more active than the Eu doped TiO_2 surface in the present investigation. It was earlier reported [62] that catalysts with mixed phases exhibited significantly higher catalytic activity than the pure anatase phase. Degussa P-25, a standard industrial photocatalyst which is composed of 70% anatase and 30% rutile, exhibited better activity owing to the better charge carrier separation in the mixed phase [62]. Therefore, the existence of mixed anatase/rutile phase formed on Eu–Ag codoped TiO_2 surface was mainly responsible for more antibacterial resistance of codoped surfaces. We considered the contribution of silver in controlling the microbial attachments. When silver ions were incorporated in to the TiO_2 matrix, they were reduced to Ag, which was proved by the XPS experiments. As suggested by the earlier literature [63–66], pre-deposited metallic silver on TiO_2 surface enhanced the photoactivity by speeding up the transport of photogenerated electrons to the outer dissolved oxygen molecules. Also, partially electrons were consumed for the reduction of Eu^{3+} to Eu^{2+} and further prevented the hole–electron pairing leading increased activity of codoped surfaces.

4. Conclusions

The Eu doped and Eu–Ag codoped TiO_2 surfaces were prepared using the sol–gel method, and their antibacterial properties were determined using TVC, epifluorescence microscopy and Raman spectroscopic techniques. It was observed that bacterial biofilm showed lesser adherence to Eu–Ag codoped surfaces than Eu doped and control surfaces. This was due to the increased photocatalysis of the codoped TiO_2 surfaces, which disintegrate the bacterial biofilm components effectively. The codopants favored the formation of anatase/rutile mixed phase and enhanced the photocatalytic activity of the surfaces. The metallic silver on TiO_2 surface enhanced the photoactivity by accelerating the transport of photogenerated electrons to oxygen molecules. Also, the increased activity of codoped surfaces was attributed to the prevention of hole–electron pairing by the consumption of electrons for the reduction of Eu^{3+} to Eu^{2+}.

References

[1] A.L. Linsebigler, G. Lu, J.T. Yates, Photocatalysis on TiO_2 surfaces: principles, mechanisms and selected results, Chemical Review 95 (1995) 735–758.
[2] S. Mo, W. Ching, Electronic and optical properties of three phase of titanium dioxide: rutile, anatase and brookite, Physical Review B 51 (1995) 13023–13032.
[3] G. Shipara Mital, T. Manoj, A review of TiO_2 nanoparticles, Chinese Science Bulletin 56 (2011) 1639–1657.
[4] A. Scalafani, L. Palmisano, M. Schiavello, Influence of the preparation methods of titanium dioxide on the photocatalytic degradation of phenol in aqueous dispersion, Journal of Physical Chemistry 94 (1990) 829–832.
[5] J. Wang, R.H. Li, Z.H. Zhang, W. Sun, X.F. Wang, Z.Q. Xing, R. Xu, X.D. Zhang, Heat treatment of nanometer anatase powder and its photocatalytic activity for degradation of acid red B dye under visible light irradiation, Inorganic Materials 44 (2008) 608–614.
[6] A. Fujishima, T.N. Rao, D.A. Tryk, Titanium dioxide photocatalysis, Journal of Photochemistry and Photobiology C: Photochemistry Reviews 1 (2000) 1–21.
[7] S. Kaewgun, B.I. Lee, Deactivation and regeneration of visible light active brookite titania in photocatalytic degradation of organic dye,

Journal of Photochemistry and Photobiology A: Chemistry 210 (2010) 162–167.
[8] T.L. Thompson Jr., J.T. Yates, Surface science studies of the photoactivation of TiO_2—new photochemical processes, Chemical Review 106 (2006) 4428–4453.
[9] P.Y. Simons, F. Dachille, The structure of TiO_2 II, a high-pressure phase of TiO_2, Acta Crystallographica 23 (1967) 334–336.
[10] X. You, F. Chen, J. Zhang, Effects of calcination on the physical and photocatalytic properties of TiO_2 powders prepared by sol–gel template method, Journal of Sol–Gel Science and Technology 34 (2005) 181–187.
[11] Y. Hu, H.L. Tsai, C.L. Huang, Phase transformation of precipitated TiO_2 nanoparticles, Materials Science and Engineering A 344 (2003) 209–214.
[12] S. Banerjee, G. Judy, P. Muraleedharan, A.K. Tyagi, B. Raj, Physics and chemistry of photocatalytic titanium dioxide: visualization of bactericidal activity using atomic force microscopy, Current Science 90 (2006) 1378–1383.
[13] A. Mills, S. Hodgen, S.K. Lee, Self-cleaning titania films: an overview of direct, lateral and remote photo-oxidation processes, Research on Chemical Intermediates 31 (2005) 295–308.
[14] K.P. Kuhn, I.F. Chaberny, K. Masholder, M. Stickler, V.W. Benz, H.G. Sonntag, L. Erdinger, Disinfection of surfaces by photocatalytic oxidation with titanium dioxide and UVA light, Chemosphere 53 (2003) 71–77.
[15] M. Kaneko, I. Okura, Photocatalysis Science and Technology. Biomedical and Medical Physics Series, Kodansha & Springer, 2002, p. 81.
[16] A. Zaleska, Doped-TiO_2: a review, Recent Patents on Engineering 2 (2008) 157–164.
[17] J. Zhu, W. Zheng, B. He, J. Zhang, M. Anpo, Characterization of Fe–TiO_2 photocatalysts synthesized by hydrothermal method and their photocatalytic reactivity for degradation of XRG dye diluted in water, Journal of Molecular Catalysis A 216 (2004) 35–43.
[18] J.C.S. Wu, C.H. Chen, A visible-light response vanadium-doped titania nanocatalyst by sol–gel method, Journal of Photochemistry and Photobiology A 163 (2004) 509–515.
[19] X.Z. Li, F.B. Li, Study of Au/Au^{3+}–TiO_2 photocatalysts towards visible photooxidation for water and wastewater treatment, Environmental Science and Technology 35 (2001) 2381–2387.
[20] X.Z. Li, F.B. Li, The enhancement of photodegradation efficiency using Pt–TiO_2 catalyst, Chemosphere 48 (2002) 1103–1111.
[21] M.S. Lee, S.S. Hong, M. Mohseni, Synthesis of photocatalytic nanosized TiO_2–Ag particles with sol–gel method using reduction agent, Journal of Molecular Catalysis A 242 (2005) 135–140.
[22] J.O. Carneiro, V. Teixeira, A. Portinha, L. Dupak, A. Magalhaes, P. Coutinho, Study of the deposition parameters and Fe-dopant effect in the photocatalytic activity of TiO_2 films prepared by dc reactive magnetron sputtering, Vacuum 78 (2005) 37–46.
[23] M.P. Seabra, I.M. Miranda Salvado, J.A. Labrincha, Pure and (zinc or iron) doped titania powders prepared by sol–gel and used as photocatalyst, Ceramics International 37 (2011) 3317–3322.
[24] C. Chaisuk, A. Wehatoranawee, S. Preampiyawat, S. Netiphat, A. Shotipruk, J. Panpranot, B. Jongsomjit, O. Mekasuwandumrong, Preparation and characterization of CeO_2/TiO_2 nanoparticles by flame spray pyrolysis, Ceramics International 37 (2011) 1459–1463.
[25] P. Supphasrirongjaroen, P. Praserthdam, O. Mekasuwandumrong, J. Panpranot, Impact of Si and Zr addition on the surface defect and photocatalytic activity of the nanocrystalline TiO_2 synthesized by the solvothermal method, Ceramics International 36 (2010) 1439–1446.
[26] Z. Wu, F. Dong, W. Zhao, S. Guo, Visible light induced electron transfer process over nitrogen doped TiO_2 nanocrystals prepared by oxidation of titanium nitride, Journal of Hazardous Materials 157 (2008) 57–63.
[27] K. Takeshita, A. Yamakata, T. Ishibashi, H. Onishu, K. Nishijima, T. Ohno, Transient IR absorption study of charge carriers photogenerated in sulfur-doped TiO_2, Journal of Photochemistry and Photobiology A: Chemistry 177 (2006) 269–275.
[28] J. Yu, M. Zhou, B. Cheng, X. Zhao, Preparation, characterization and photocatalytic activity of in situ N, S-codoped TiO_2 powders, Journal of Molecular Catalysis A 246 (2006) 176–184.
[29] S.Y. Treschev, P.W. Chou, T.H. Tseng, J.B. Wang, E.V. Perevedentseva, C.L. Cheng, Photoactivities of the visible light-activated mixed phase carbon-containing titanium dioxide: the effect of carbon incorporation, Applied Catalysis B 79 (2008) 8–16.
[30] A. Zaleska, J.W. Sobczak, E. Grabowska, J. Hupka, Preparation and photocatalytic activity of boron-modified TiO_2 under UV and visible light, Applied Catalysis B 78 (2007) 92–100.
[31] J. Xu, Y. Ao, D. Fu, A novel Ce, C-codoped TiO_2 nanoparticles and its photocatalytic activity under visible light, Applied Surface Science 256 (2009) 884–888.
[32] X. Yang, F. Ma, K. Li, Y. Guo, J. Hu, W. Li, M. Huo, Y. Guo, Mixed phase titania nanocomposite codoped with metallic silver and vanadium oxide: new efficient photocatalyst for dye degradation, Journal of Hazardous Materials 175 (2010) 429–438.
[33] Z.M. El-Bahy, A.A. Ismail, R.M. Mohamed, Enhancement of titania by doping rare earth for photodegradation of organic dye (direct blue), Journal of Hazardous Materials 166 (2009) 138–143.
[34] C. Wang, Y. Ao, P. Wang, J. Hou, J. Qian, Photocatalytic performance of Gd ion modified titania porous hollow spheres under visible light, Materials Letters 64 (2010) 1003–1006.
[35] Y.H. Xu, C. Chen, X. Yang, X. Li, B. Wang, Preparation, characterization and photocatalytic activity of the neodymium-doped TiO_2 nanotubes, Applied Surface Science 255 (2009) 8624–8628.
[36] C. Wang, Y. Ao, P. Wang, J. Hou, J. Qian, S. Zhang, Preparation, characterization, photocatalytic properties of titania hollow sphere doped with cerium, Journal of Hazardous Materials 178 (2010) 517–521.
[37] W. Xiaohong, Q. Wei, D. Xianbo, W. Yang, L. Huiling, J. Zhaohua, Photocatalytic activity of Eu-doped TiO_2 ceramic films prepared by microplasma oxidation method, Journal of Physical Chemistry of Solids 68 (2007) 2387–2393.
[38] W. Luo, R. Li, G. Liu, R.M. Antonio, X. Chen, Evidence of trivalent europium incorporated in anatase TiO_2 nanocrystals with multiple site, Journal of Physical Chemistry C 112 (2008) 10370–10377.
[39] J. Xu, Y. Ao, D. Fu, C. Yuan, A simple route for the preparation of Eu, N-codoped TiO_2 nanoparticles with enhanced visible light-induced photocatalytic activity, Journal of Colloid and Interfacial Science 328 (2008) 447–451.
[40] C. Chi, J. Choi, Y. Jeong, O.Y. Lee, H.J. Oh, Nitrogen and europium doped TiO_2 anodized films with applications in photocatalysis, Thin Solid Films 519 (2011) 4676–4680.
[41] S. Ramya, R.P. George, R.V. Subba Rao, R.K. Dayal, Effect of biofouling on anodized and sol–gel treated titanium surfaces: a comparative study, Biofouling 26 (2010) 883–891.
[42] A. Hreniak, M. Nyk, D. Hreniak, W. Stręk, L. Kępiński, J. Misiewicz, K. Maruszewski, Optical properties of Eu(III) doped nanocrystalline films of TiO_2, Material Science—Poland 22 (2004) 227–234.
[43] J.F. Moulder, W.F. Stickle, P.E. Sobol, K.D. Bomben, J. Chastain, in: J. Chastain, R.C. King Jr. (Eds.), Handbook of X-Ray Photo-Electron Spectroscopy, ULVAC-PHI Inc., Chigasaki, Japan, 1995.
[44] APHA, Standard methods for the examination of water and waste water, Washington DC, 1989, pp. 182–184.
[45] T.C. Mah, G.A. O'Toole, Mechanisms of biofilm resistance to antimicrobial agents, Trends in Microbiology 9 (2001) 34–39.
[46] H. Long, G. Yang, A. Chen, Y. Li, P. Lu, Growth and characteristics of laser deposited anatase and rutile TiO_2 films on Si substrates, Thin Solid Films 517 (2008) (2008) 745–749.
[47] R.S. Ningthoujam, V. Sudarsan, R.K. Vatsa, R.M. Kadam, Jagannath, A. Gupta, Photoluminescence studies on Eu doped TiO_2 nanoparticles, Journal of Alloys and Compounds 486 (2009) 864–870.
[48] Q.G. Zeng, Z.J. Ding, Z.M. Zhang, Synthesis, structure and optical properties of Eu^{3+}/TiO_2 nanocrystals at room temperature, Journal of Luminescence 118 (2006) 301–307.

[49] Y. Zhang, H. Zhang, Y. Xu, Y. Wang, Significant effect of lanthanide doping on the texture and properties of nanocrystalline mesoporous TiO_2, Journal of Solid State Chemistry 177 (2004) 3490–3498.
[50] B.D. Cullity, S.R. Stock, Elements of X-Ray Diffraction, 3rd Edn, Prentice-Hall, Englewood Cliffs, NJ, 2001 167–171.
[51] G. Liu, X. Wanga, Z. Chen, H. Cheng, G.Q. Lu, The role of crystal phase in determining photocatalytic activity of nitrogen doped TiO_2, Journal of Colloid and Interface Science 329 (2009) 331–338.
[52] M. Pal, U. Pal, J.M. Gracia, Y. Jiménez, F. Pérez-Rodríguez, Effects of crystallization and dopant concentration on the emission behavior of TiO_2:Eu nanophosphors, Nanoscale Research Letters 7 (2012) 1–12.
[53] Z. Zhao, Q.G. Zeng, Z.M. Zhang, Z.J. Ding, Optical properties of Eu^{3+}/TiO_2 nanocrystalline under high pressure, Journal of Luminescence 122–123 (2006) 862–865.
[54] A.K. Parchur, R.S. Ningthoujam, S.B. Rai, G.S. Okram, R.A. Singh, M. Tyagi, S.C. Gadkari, R. Tewari, R.K. Vatsa, Luminescence properties of Eu^{3+} doped $CaMoO_4$ nanoparticles, Dalton Transactions 40 (2011) 7595–7601.
[55] R.S. Ningthoujam, V. Sudarsan, S.V. Godbole, L. Kienle, S.K. Kulshreshtha, SnO_2:Eu^{3+} nanoparticles dispersed in TiO_2 matrix: improved energy transfer between semiconductor host and Eu^{3+} ions for the low temperature synthesized samples, Applied Physics Letters 90 (2007) 173113–173116.
[56] X. Tan, M. Fang, J. Li, Y. Lu, X. Wang, Adsorption of Eu (III) onto TiO_2: effect of pH, concentration, ionic strength and soil fulvic acid, Journal of Hazardous Materials 168 (2009) 458–465.
[57] S. Ramya, R.P. George, R.V. Subba Rao, R.K. Dayal, Detection of algae and bacterial biofilms formed on titanium surfaces using micro-Raman analysis, Applied Surface Science 256 (2010) 5108–5115.
[58] P.C. Lee, D. Meisel, Adsorption and surface-enhanced Raman of dyes on silver and gold sols, Journal of Physical Chemistry 86 (1982) 3391–3395.
[59] M.L. Laucks, A. Sengupta, K. Junge, E.J. Davis, B.D. Swanson, Comparison of psychro-active arctic marine bacteria and common mesophillic bacteria using surface-enhanced Raman spectroscopy, Applied Spectroscopy 59 (2005) 1222–1228.
[60] Y. Zheng, P.R. Carey, B.A. Palfey, Raman spectrum of fully reduced flavin, Journal of Raman Spectroscopy 35 (2004) 521–524.
[61] K.C. Schuster, E. Reese, E. Urlaub, J.R. Gapes, B. Lendl, Multidimensional information on the chemical composition of single bacterial cells by confocal Raman microspectroscopy, Analytical Chemistry 72 (2000) 5529–5534.
[62] D.M. Blake, P.C. Maness, Z. Huang, E.J. Wolfrum, W.A. Jacoby, J. Huang, Application of the photocatalytic chemistry of titanium dioxide to disinfection and the killing of cancer cells, Separation and Purification Methods 28 (1999) 1–50.
[63] R. Kumar, H.M. Unstedt, Silver ion release from antimicrobial polyamide/silver composites, Biomaterials 26 (2005) 2081–2088.
[64] V. Vamathevan, R. Amal, D. Beydoun, G. Low, S. McEvoy, Photocatalytic oxidation of organics in water using pure and silver-modified titanium dioxide particles, Journal of Photochemistry and Photobiology A 148 (2002) 233–245.
[65] E. Szabó-Bárdos, H. Czili, A. Horváth, Photocatalytic oxidation of oxalic acid enhanced by silver deposition on a TiO_2 surface, Journal of Photochemistry and Photobiology A 154 (2003) 195–201.
[66] M.A. Behnajady, N. Modirshahla, M. Shokri, B. Rad, Enhancement of photocatalytic activity of TiO_2 nanoparticles by silver doping: photodeposition versus liquid impregnation methods, Global NEST Journal 10 (2008) 1–7.